Report submitted for **HPC Challenge 2009, Category C: PARALLEL SPEEDUP**

Project Title: **Computational Fluid Dynamics Analysis on Drag Reduction for Grid-Fin Configurations**

Project Member Names and Department:
Yan Zeng
Temasek Laboratories, National University of Singapore, Singapore, 119260, Singapore

1. Description of project

1.1 Background

A grid fin, also called a lattice fin, is an unconventional aerodynamic control device consisting of an outer frame with internal intersecting grid frameworks of small chord. Unlike conventional fins that are aligned parallel to the direction of the airflow, a grid fin is arranged perpendicular to the flow allowing the oncoming air to pass through the lattice grid cells. The improved maneuverability offered by grid fins at high supersonic speeds and high angles of attack has attracted much attention to grid fins in recent years.

Flow passing through grid fins is quite complex due to their complicated configurations. Thus computational methods are considered as useful tools to solve the complete flow field. Recently more research efforts have been taken to investigate the aerodynamic characteristics of these devices in order to optimize their performance by using computational fluid dynamics (CFD) analysis.

Chen et al. [1] conducted numerical investigations of a vehicle configuration with grid fins by using the NPARC code of NASA. The issue of the optimum grid fin size, in terms of both the panel thickness and the frontal shape was addressed. Lin et al. [2] performed computations of turbulent flows past a grid fin alone and fin-body combinations at Mach numbers of 2.5 and 0.7. The computations provided the detailed flow fields including Mach-number contours, pressure contours, streamline patterns and the integrated aerodynamic coefficients. DeSpirito et al. [3, 4] conducted CFD studies on grid fins by using the commercial CFD code FLUENT which presented the first known published viscous CFD computations of grid fins. The simulations successfully predicted the flow structures around the fin in the separated-flow region at higher angles of attack. The objective was to investigate the advantages of grid fins over conventional controls when employed on highly maneuverable vehicles. Hughson et al. [5] conducted computational fluid dynamics (CFD) studies to investigate the flow fields over the vehicle-grid fin configuration tested by Abate [6]. The CFD results showed the presence of choked flow within the cells and the formation of a normal shock behind the grid fin at transonic Mach numbers.

An important aerodynamic characteristic of grid fins concerns drag, which could be an advantage or a disadvantage depending on the speed of the airflow. At low subsonic speeds, the drag and control effectiveness of a lattice fin are about the same as those of a conventional fin, as the thin shape of the lattice walls creates very little disturbance in the flow of air passing through. However, the same behavior does not hold true at Mach numbers near 1. In this transonic regime, the flow inside the cells chokes thus reducing the flow rate through the fin, and the lattice effectively acts as an obstacle to the flow. Due to the formation of normal shock waves, the drag increases significantly and the control effectiveness decreases. When the speed goes higher, the normal shock is swallowed and shock waves are instead formed off the leading edges of the lattice with an oblique angle. The oblique angle decreases with increasing the Mach number until the shock passes through the structure without intersecting it. In this regime, the drag and the control effectiveness of grid fins are superior.

1.2 Significance and impact of research

Thus the main objective of the present CFD study is to find a way to overcome the high drag of the grid fins in the transonic flow regime. An improved configuration, sweptback grid fins, is proposed to

reduce the transonic choking without compromising the control effectiveness of the grid fin. The physics of the shock interaction and choking behavior within the cells of both normal and sweptback grid fins are also examined under both transonic and supersonic conditions.

The significance of this research is to propose a new grid-fin design for improved performance while keeping the control effectiveness of the grid fin almost unchanged. The framework of the baseline grid fin is sweptback along the chord-wise direction and the overall effect is that the cubic cells located within the middle of the grid fin no longer act as "complete" nozzles such as that formed by the baseline grid fin cells. Thus the new configuration can reduce the high flow resistance caused by the baseline gird fins, so does the drag force. Once the flow resistance and drag are reduced, the vehicle may have performance enhancement with faster speed and longer distance for flying. The objectives of energy saving and efficiency enhancement can also be achieved. In addition, the new design is quite cost-effective without any additional input power.

1.3 Problem size and complexity

1.3.1 Grid fin configuration

The geometry investigated by Abate et al. [6] and Hughson et al. [5] is selected as the baseline, which consists of a 3-caliber tangent ogive nose, 13-caliber long cylindrical afterbody with four grid fins mounted in a cruciform orientation, as shown in Figure 1. The pitch axis of the grid fins is located 1.5-caliber from the rear of the cylinder. The grid fin has rectangular shaped outer frames, with the span (*s*), height (*h*) and chord (*c*) of 0.75-, 0.333- and 0.118-caliber respectively. The web thickness (*t*) is 0.007-caliber and the model reference diameter (*D*) is 1 inch. The details about the configuration have also been described in the previous study [7].

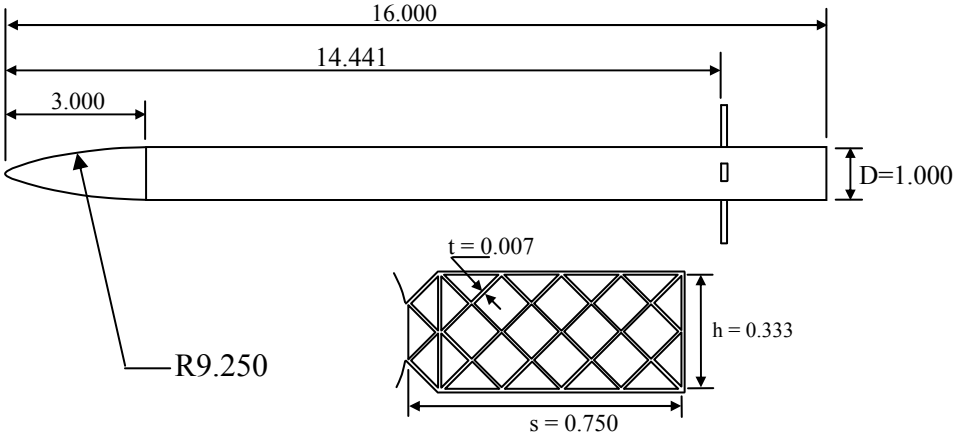
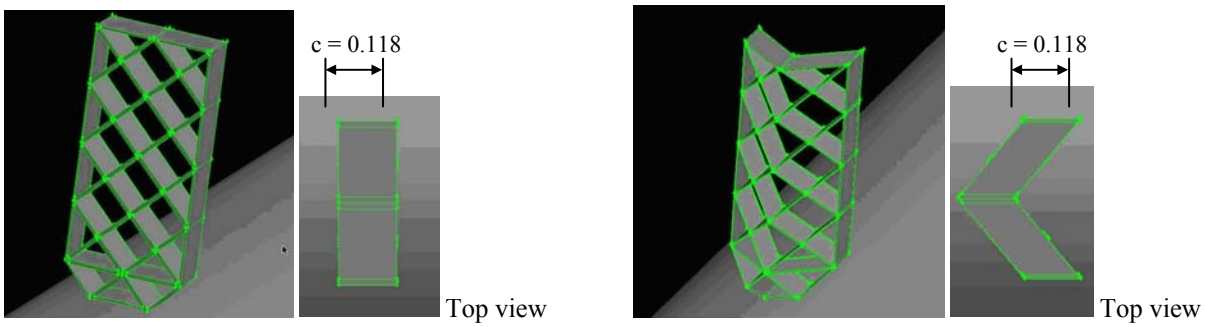


Figure 1 Schematic of the ogive cylinder with grid fin configuration



(a) Baseline model **(b) Sweptback model**

Figure 2. Schematic of the baseline and sweptback grid fin configurations

Figure 2(a) schematically shows the baseline lattice grid fin three-dimensionally. The schematic of the proposed improved sweptback grid fin configuration is shown in Figure 2(b), with the frameworks of grid cells swept back along chord direction whereas the same projected structure and dimensions as those of the baseline lattice grid fin shown in Figure 1. The sweptback grid fins are also mounted in a cruciform orientation on the same ogive cylinder and located at the same position comparably with the baseline grid fin. The sweptback angle, α is 30° in the present study.

1.3.2 Mesh generation

The most challenging part in CFD simulations of the flow over a vehicle with grid fins is to create mesh with satisfactory quality. Due to the complicated geometry of fins, the structured grid generation requires a lot of manpower. Even if the structured grid can be generated with a lot of time, the quality of the grid distribution may not be good, especially within the region of the grid fins. Thus, in the present study, GAMBIT, supplied in the CFD software FLUENT suite, was used to generate the unstructured grid. To take the advantages of model symmetry at zero angle of attack, only a quarter of the vehicle with grid fin was considered in the present CFD study.

Using the wall function in FLUENT, a boundary layer mesh was used near the vehicle body and fin surfaces. The spacing between the first grid point and the surface is 0.001D with a growth factor of 1.2 and at least 9 points distributed within the boundary layer corresponding to the Reynolds number used by the free flight test of Abate et al. [6]. In order to enhance the mesh quality, the whole computational domain is divided into three sections comprising respectively of the fin, transition section and the remaining section.

Figures 3(a) and 3(b) show the enlarged grid in the upstream nose and downstream base regions on the symmetry surface respectively so as to show the full computational grid near the cylinder body. Figures 3(c) and 3(d) show the enlarged view of the grid on the slices of the fin front surface and symmetry surface respectively. An unstructured triangular mesh was used for the fin section (Fig. 3c). Grids within the fin section are highly clustered to the cell surface as well as the leading and trailing edges of each cell spar. Three transitional sections were located on the top of, before, and after the fin section respectively. Within these transitional sections, the very fine mesh in the fin can be gradually merged into the coarse mesh in the remaining section, thus significantly reducing the total grid number for the whole computational domain. As seen in Fig. 3(d), T-Grid type was used within these transitional sections. The advantage of this type of grid is the unrestricted usage of grid number and grid type for different surfaces, while the disadvantage is that the volume mesh depends strongly on the mesh quality of each surface, which gives a lot of trouble in the grid generation process. In the remaining section, which consists mainly of the ogive cylinder body, a structured grid was used, as shown in Figs. 3(a) and 3(b). The upstream and downstream boundaries are located 12-calibers away from the nose and tail of the cylinder body, and 16-calibers radially from the cylinder surface. To control the grid-element number and enhance computation efficiency, different grid types have been used in different sections and in total 13 grid interfaces were applied to connect these sections. Totally there are 78 volume entities with the grid-element number around 1.5 million, for the whole 3D computational domain. The memory usage is more than 3GB for each case, which is quite large and thus parallel computing is necessary to speed up the computation.

For the improved configuration, sweptback grid fin, the grid topology is similar to that for the normal grid fin, and thus it is not shown here for the sake of brevity. However, the grid generation is even more challenging because the configuration now is even more complex. Totally, there are 85 volume entities with the grid-element number around 1.5 million for a quarter of the whole model.

1.3.3 Flow solver and boundary conditions

CFD software FLUENT was chosen as the flow solver to model the flow phenomena. The governing equations were solved by using finite volume method with unstructured-grid. Spalart-Allmaras one equation turbulent model was used for simulations. Second-order, upwind discretization scheme was employed for flow variables and turbulent viscosity. Implicit, density-based solver was adopted for high speed compressible flow investigated in this study.

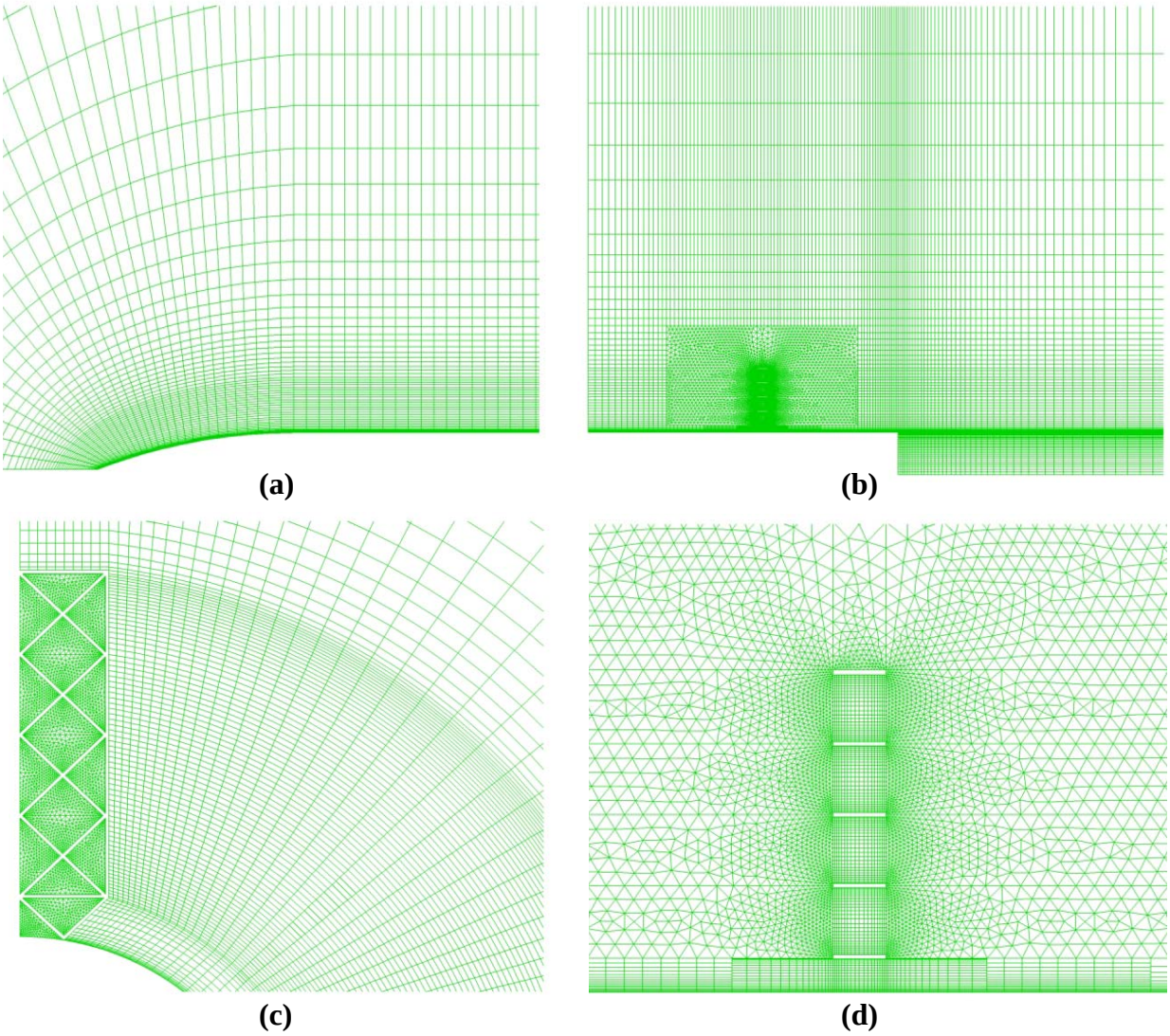


Figure 3 Mesh topology for the vehicle with baseline grid fins: (a) upstream nose region at the symmetry surface along the body axis, (b) downstream wake region at the symmetry surface along the body axis, (c) fin surface perpendicular to the body axis, (d) fin region at the symmetry surface along the body axis

The free-stream Mach number ($M\infty$) is set at 0.817 – 2.0 and Reynolds number (Re_D) is 4.69 - 11.48 x 10^5 (based on diameter D) for comparison with the ARF free flight test data. The free-stream static pressure and temperature is 1 atm and 295 K respectively. The angle of attack is zero. Far-field pressure boundary conditions were applied for the outer radial boundary; symmetric conditions for surfaces of symmetry, and non-slip conditions for all solid surfaces. At the downstream outflow boundary a user-defined function is compiled to extrapolate all the flow quantities from the interior grid points. Maximum residuals were reduced at least 3 orders of magnitude for all the variables to confirm the global convergence of the simulations.

To validate the present numerical approach, the computed drag coefficients of the present CFD study under transonic and supersonic flows with Mach numbers 0.8-2 are compared with the CFD data provided by Hughson et al. [5]. The present results and previous CFD results agree well, within the error of 4%. The good agreement indicates that the present numerical method is accurate enough to capture the flow phenomena and physics of the flows over vehicles with grid fins.

2. Results and Discussion

2.1 Comparison of aerodynamic drag coefficients between baseline and sweptback models

The present numerical method is employed to simulate the flows over the vehicle with sweptback grid fin configurations in the transonic and supersonic flows with Mach numbers of 0.8-2.0. Similarly, the aerodynamic drag coefficients C_D are integrated along the vehicle model body and sweptback grid fin surfaces. The reference length and area are the same as those for the baseline model.

The aerodynamic drag coefficients under the same Mach number between the baseline and sweptback the model are calculated and compared, as shown in Tables 1 and 2. Table 1 shows the difference of the overall drag coefficients on the whole body for the two models, and Table 2 shows the difference of the drag coefficients on the fin part.

The comparisons in Tables 1 and 2 clearly show that the use of sweptback gin fin configurations is beneficial for drag reduction. At all the Mach number of 0.905, 1.045, 1.19, 1.332 and 2.0 investigated currently, by using the improved sweptback fin configurations, Table 1 shows that that the overall drag reduces around 4.46% - 6.38%, compared with that by using the baseline grid fins. The conditions for the drag reduction on the fin part are even better, as shown in Table 2, with approximately 12.46% - 13.29% reduction for the improved sweptback model compared with the baseline model. The reason for the drag reduction is believed to be due to the sweptback framework of the fin, causing the flow not perpendicular to the fin cell and the reduction in the flow resistance. Thus the flows can pass the grid fin cells more easily and the flow field becomes more uniform before and after the grid fin cells, and flow chokes inside the fin cells are reduced or avoided, which will be seen clearly in the Figures 4 and 5 as shown later.

Table 1 Overall drag coefficient (C_D) for models with baseline and sweptback grid fins

Freestream Mach number	Baseline rid fin	Sweptback grid fin	Drag reduction
0.905	0.784	0.734	6.38 %
1.045	0.922	0.870	5.64 %
1.190	0.896	0.856	4.46 %
1.332	0.841	0.796	5.35 %
2.0	0.700	0.662	5.43 %

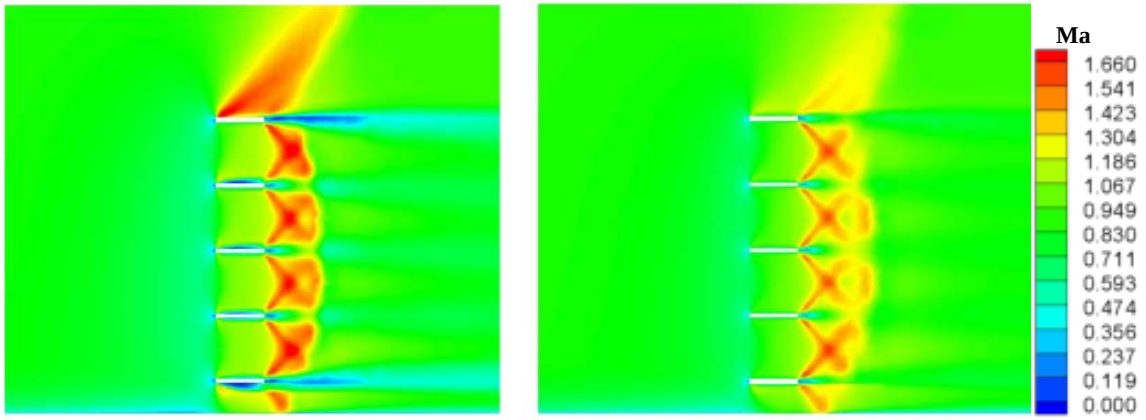
Table 2 Drag coefficient on fin part ($C_{D,fin}$) for baseline and sweptback grid fins

Freestream Mach number	Baseline grid fin	Sweptback grid fin	Drag reduction
0.905	0.504	0.437	13.29 %
1.045	0.448	0.392	12.50 %
1.190	0.406	0.353	13.05 %
1.332	0.384	0.332	13.54 %
2.0	0.345	0.302	12.46 %

2.2 Flow characteristics for baseline and sweptback models

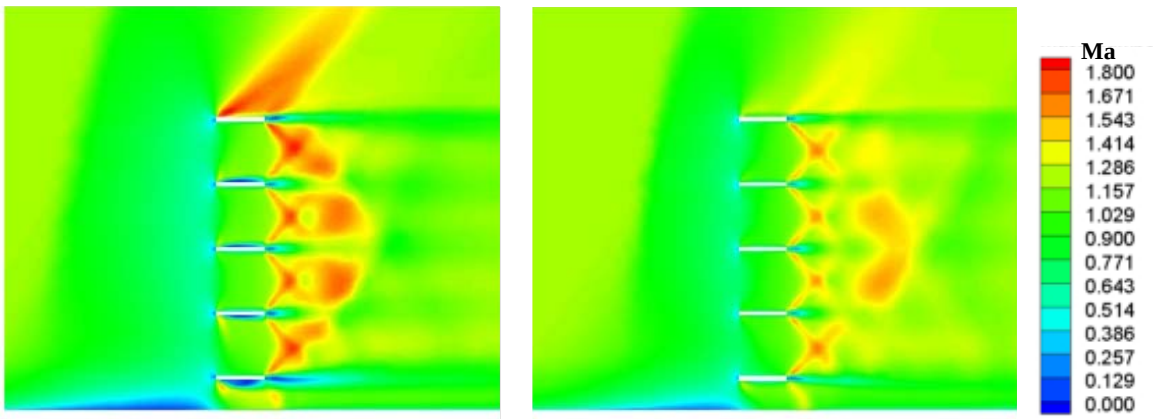
The flow fields through the baseline and sweptback grid fin configurations are fairly complex. The Mach number (*Ma*) and pressure coefficient (C_p) contours on symmetry surface are shown in Figures 4 and 5 respectively, at the freestream Mach numbers 0.905, 1.19 and 2.0, for these two configurations. The webs have blunt leading edges to cause a rapid expansion as the flow passes by the corner. The boundary layer, which grows from the leading edge, coupled with stagnated flow in the web spar junctures causes the decrease in the flow area, leading to flow acceleration and related choke flow phenomena. As shown in Figures 4 and 5, for the baseline grid fin configuration, choking flows are observed inside the fin cells

with high Mach number and low pressure. The region with even higher Mach number and lower pressure caused by expansion wave is formed at the trailing edge of the web. However, for the sweptback of the grid fin (also shown in Figures 4 and 5), it is found that the flow resistance is reduced, the flow field is more uniform and the region with high Mach number and lower pressure disappears.



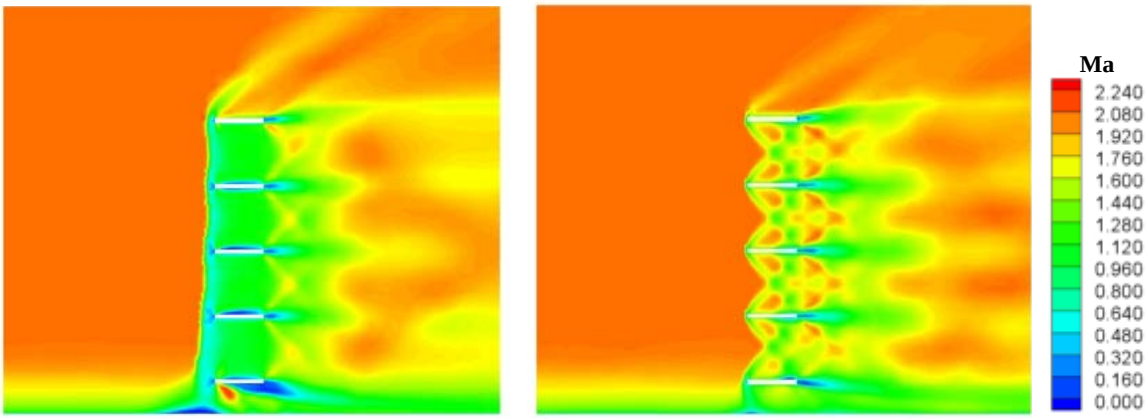
(i) Baseline model **(ii) Sweptback model**

(a) Ma = 0.905



(i) Baseline model **(ii) Sweptback model**

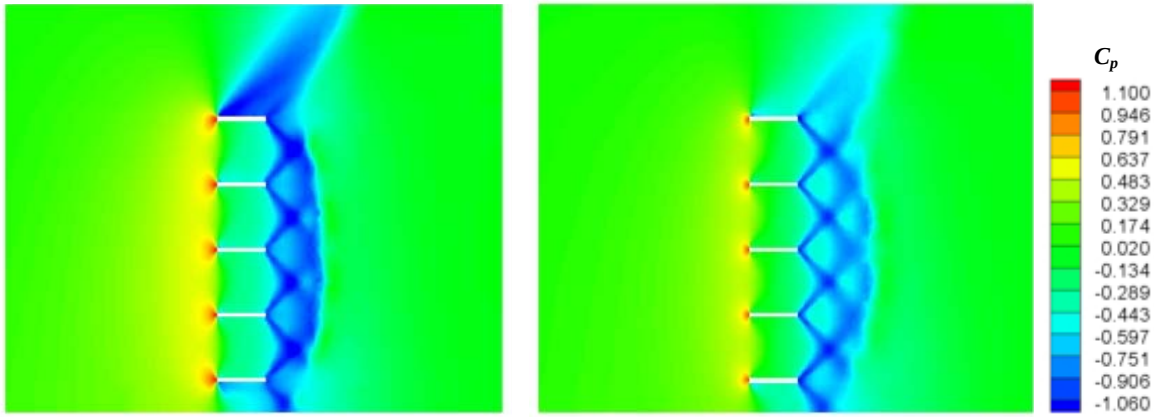
(b) Ma = 1.19



(i) Baseline model **(ii) Sweptback model**

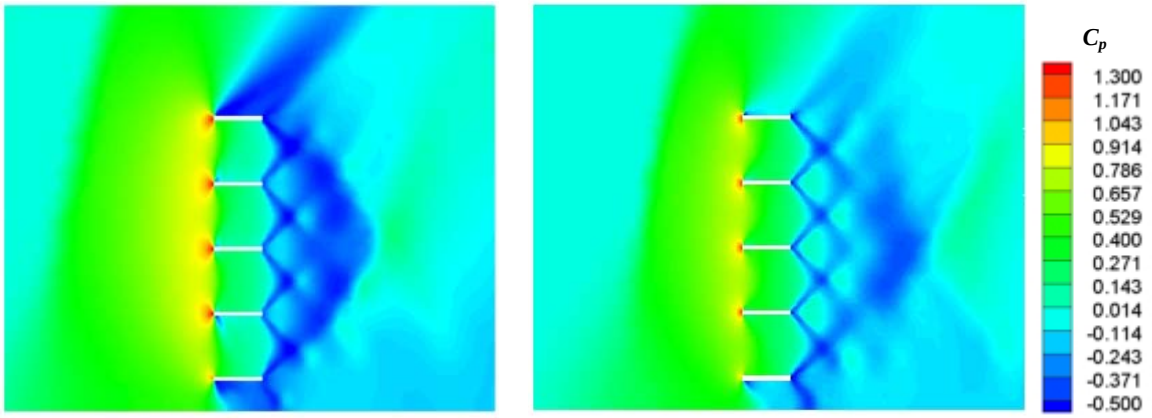
(c) Ma = 2.0

Figure 4 Mach number contours for the baseline and sweptback models at symmetry surface for freestream Ma=0.905, 1.19, and 2



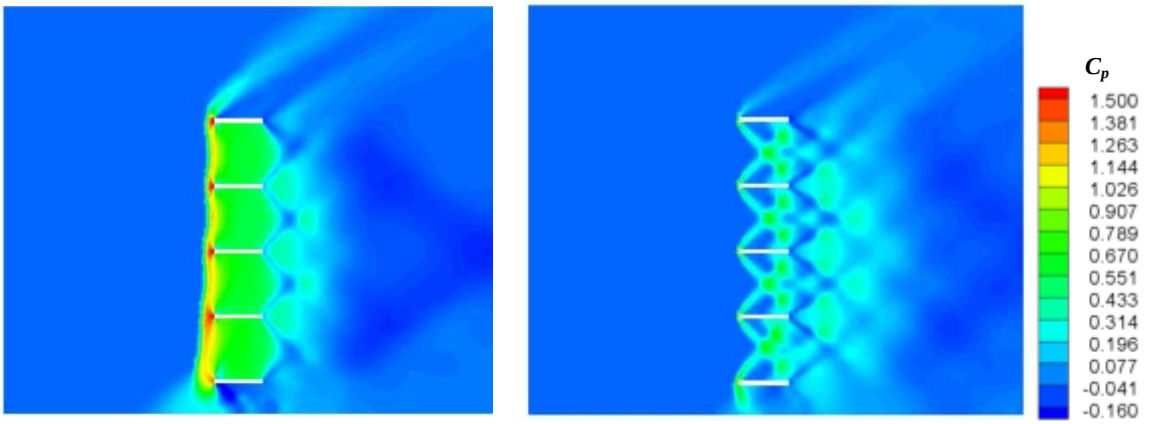
(i) Baseline model **(ii) Sweptback model**

(a) Ma = 0.905



(i) Baseline model **(ii) Sweptback model**

(b) Ma = 1.19



(i) Baseline model **(ii) Sweptback model**

(c) Ma = 2.0

Figure 5 Pressure coefficient contours for the baseline and sweptback models (with swept back in 80ml) at symmetry surface for freestream Ma=0.905, 1.19, and 2

For the baseline grid fin configuration, when the freestream Mach number is 0.905, a three-dimensional diamond wave pattern is found to develop in the region behind the lattice cells (Figures 4a i) due to the interaction of the expansion wave. When Mach number increases to 1.19, a very week local shock wave is formed in front of the leading edge of the web, but it is far away enough so that the flow

pattern is relatively unchanged (Figures 4b i). With Mach number further increasing to 2.0 (Figures 4c i), a strong normal shock wave is formed in front of the grid fin and slightly weaker expansion wave is formed at the trailing edge of the web. The cell flow accelerates quickly and uniformly so that the choking shock seems to be swallowed.

While for the sweptback grid fin, when the freestream $M\infty$ = 0.905, the original three-dimensional diamond wave pattern behind the lattice cells (Figure 4a i) is now reduced in Mach number magnitude and pattern area (Figure 4a ii), resulting from the reduced interaction of the expansion wave. When Ma increases to 1.19, there is still a very week local shock wave formed before and closer to the leading edge of the web (Figures 4b ii). The flow pattern also shows the diminishment of the expansion wave and that of the interaction of the expansion wave behind the fin cells. When Mach number further increases to 2.0, the strong shock wave in front of the grid fin now goes into the fin cells, forming the oblique shock wave inside, and still slightly weaker expansion wave formed at the trailing edge of the web (Figures 4c ii). The observations gathered here proves the reduction in flow chokes and drag coefficients, by use of the sweptback grid fin configuration.

From the contours of pressure coefficients as shown in Figure 5, it is also clearly seen that for the baseline grid fin configuration, the pressure gradient is high when flows passes through the normal grid fins, while for the sweptback grid fin configuration, the pressure gradient is decreased, indicating the reduction in the flow resistance. The different flow behaviors over the baseline and sweptback gird fin configurations from these figures (Figures 4 and 5) further elucidating the favorable function of using sweptback grid fins to reduce flow resistance, flow choking and subsequently drag force.

3. Description of Speedup achieved and Parallelization creativity

For the cases running in FLUENT, the mesh must be divided into smaller, evenly sized partitions so as to make the case be run in parallel. Each FLUENT process, called a compute node, will solve on a single partition, and information will be passed back and forth across all partition interfaces. FLUENT solver allows parallel processing on a dedicated parallel machine, or a network of workstations running Linux, UNIX, or Windows [8].

In FLUENT, when the parallel solver is used, the grid needs to be subdivided into groups of cells that can be solved on separate processors. For the present grid fin cases, after the case file is read into FLUENT, the panel command "parallel → partition" is applied to make FLUENT automatically partition the grid according to the partition settings and FLUENT will print the active partition statistics in the console. The present cases have been run in two different clusters: Atlas3 and Atlas4. The partition number is set as the CPU-core number that the case will use later, which has been set differently to be 1, 4, 8, 10 and 12 for the clusters Atlas3 and Atlas4. Different clusters with different CPU-core numbers were used to compare the different computational speed.

Before presenting the speedup results by using parallel processing, several important parameters must be defined first as below:

$$SP_N = T_1 / T_N \qquad (1)$$

$$EF_N = T_1 / \left(N \cdot T_N \right) \qquad (2)$$

where SP_N is the speedup factor, EF_N is the efficiency of the present FLUENT cases, N is the number of CPU-core, T_1 is the wall clock time of the sequential algorithm, and T_N is the wall clock time of the parallel algorithm with P CPU-core.

Table 3 summarizes the different computation time (wall clock time) for 100 iterations of each case by using different CPU cores in different clusters of Atlas3 and Atlas4. Figure 6 shows the parallel speedup factor and efficiency using different number of CPU-cores for both nodes.

Table 3 shows that the computational time decreases significantly with increasing the CPU-cores. For different clusters, the computational time is also different even for the same CPU-core number. For the computation in single CPU, cluster Atlas3 shows faster speed compared with cluster Atlas4. However, cluster Atlas4 shows faster speed when 4 or 8 CPU-core are used, as seen in Table 3 clearly. Figure 6 shows the speedup data by calculating the speedup factor and efficiency in different clusters. From Figure

6 (a), it is shown that cluster Atlas4 has larger speedup factor for the same multi-CPU-core number used compared with cluster Atlas3. For 4 and 8 CPU-core used, the speedup factors in cluster Atlas4 are around 3.5 and 5.1, much higher than those in cluster Atlas3 of around 2.1 and 3.1 respectively. This indicates that the efficiency of parallel processing in cluster Atlas4 is higher than that in cluster Atlas3, which is also observed in Figure 6 (b). In Figure 6 (b), two lines show the computation efficiency for different CPU-core numbers in clusters Atlas3 and Atlas4. The efficiency line for cluster Atlas3 is below the line for cluster Atlas4, showing higher computation efficiency for cluster Atlas4 for the same CPU-core used. The efficiency for 4 and 8 CPU-cores used in cluster Atlas4, the efficiencies are 87% and 64%, which are higher than those in cluster Atlas3 of approximately 53% and 38% respectively.

Table 3 Comparison of wall clock time for different CPU-core numbers

Cluster Atlas3					
CPU-core numbers	1	4	8	10	12
Wall Clock Time (s)	4759	2237	1559	1434	1400
Cluster Atlas4					
CPU-core numbers	1	4	8	10	12
Wall Clock Time (s)	5714	1635	1120	951	876

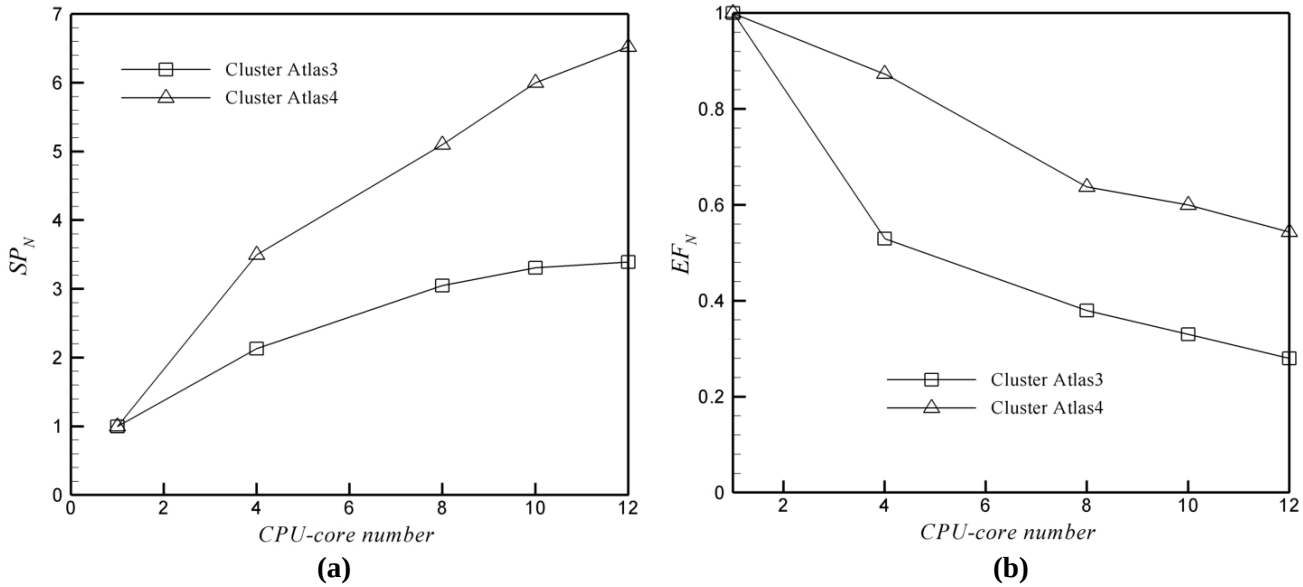


Figure 6 Speedup data: (a) speedup factor, (b) efficiency of the present FLUENT parallelization in different clusters

For the grid-fin simulations in the present study, it usually takes 5 to 7 days to get converged results for each case by using 8 CPU-cores in cluster Atlas4, depending on the system load. Based on the speedup data shown in Table 3 and Figure 6, it can be estimated that it needs to run approximately 25 to 35 days to finish one case if only use a Single CPU-core in cluster Atlas4, which may not be bearable if a large amount of cases need to run within the limited time. Thus the parallel processing has significantly speeded up the present study and made the completion of the project within the limited time become true.

4. Conclusion

A normal choke usually forms at the back of the lattice grid cells at transonic Mach numbers, causing a significant increase in drag force. The present study proposed an improved sweptback grid fin, to reduce the transonic choking, so as to reduce the drag. Viscous computational fluid dynamic (CFD) simulations were performed to investigate flows over an ogive cylinder with baseline and sweptback grid fins in transonic and supersonic flows of Mach number 0.8-2.0, at zero angle of attack. The present simulations show that the choke can be reduced by using the sweptback grid fins. The sweptback grid fins are found to be beneficial in the drag reduction, with approximately 5% reduction for the overall drag, and nearly 12% reduction for the drag on the fin part, for all the Mach numbers investigated in the present study.

Due to a complicated geometry with a large amount of grid elements, parallel processing was used to speed up the computation. Different numbers of CPU-cores were used to compare the different computation time and the parallel efficiency. It is seen that with parallel processing of 8-CPU cores, the computation time is speedup to 1/5 of that using single CPU. For the present cases which usually need to run 5-7 days in cluster Atlas4 by using 8-CPU cores, 25-35 days may be needed to finish one case for single CPU running, which is quite long and may obstruct the completion of the project in a limited time. Thus FLUENT parallelization actually significantly speeds up the simulations and enhances the efficiency, saving a lot of time in computation to complete the project within a limited time.

References

1. Chen, S., Khalid, M., Xu, H., and Lesage, F., "A comprehensive CFD investigation of grid fins as efficient control surface devices," AIAA-2000-987, *38th Aerospace Sciences Meeting and Exhibit*, Reno, NV, Jan. 10-13, 2000.

2. Lin, H., Huang, J., and Chieng, C., "Navier-Stokes Computations for Body/Cruciform Grid fin Configuration," AIAA-2002-2722, *20th AIAA Applied Aerodynamics Conference*, St. Louis, Missouri, June 24-26, 2002.

3. DeSpirito, J., and Sahu, J., "Viscous CFD Calculations of Grid Fin Aerodynamics in the Supersonic Flow Regime," AIAA-2001-257, January 2001.

4. DeSpirito, J., Edge, H. L., Weinacht, P., and Sahu, J., "Computational Fluid Dynamics Analysis of a Vehicle with Grid Fins," Journal of Spacecraft and Rockets, Vol.38, No.5, 2001, pp. 711-718.

5. Hughson, M. C., Blades, E. L., and Abate, G. L., "Transonic Aerodynamic Analysis of Lattice Grid Tail Fin Vehicles," AIAA-2006-3651, June 2006.

6. Abate, G., Winchenbach, G., and Hathaway, W., "Transonic aerodynamic and scaling issues for lattice fin projectiles tested in a ballistic range," in proceedings of the 19th International Symposium of Ballistics, pp. 413-420, 7-11 May 2001, Interlaken, Switzerland.

7. Zeng, Y., Cai, J. S., Debiasi, M., and Chng, T. L. "Numerical Study on Drag Reduction for Grid-Fin configurations," AIAA-2009-1105, the 47th AIAA Aerospace Sciences Meeting and Exhibit, Orlando, Florida, January 5-8, 2009.

8. FLUENT 6.3 User Guide, Fluent, Inc., Lebanon, NH, 2006.